Combining unmanned aerial vehicle and multispectral Pleiades data for tree species identification, a prerequisite for accurate carbon estimation

Agbor Esong Effiom,[a,*] Louise M. van Leeuwen,[b] Panagiotis Nyktas,[b] Jefferson Adetokunbo Okojie,[a] and Jana Erdbrügger[a]

[a]University of Twente, Faculty of Geo-information Science and Earth Observation Alumini, Enschede, The Netherlands

[b]University of Twente, Faculty of Geo-information Science and Earth Observation-Natural Resources, Enschede, The Netherlands

Abstract. Forest carbon estimation currently largely relies on remote sensing techniques in combination with field measurement. High-resolution images, which are commonly utilized for carbon estimation, are not readily available, and their cost prohibits communities from reaping the benefits of maintaining their forest under the UN reducing emissions from deforestation and forest degradation program. Our study explores the combination of readily available and relatively cheaper unmanned aerial vehicle (UAV) (4-cm resolution) and multispectral Pleiades (50-cm resolution) images for species classification robustness in view for carbon estimation through object-based image analysis. The images are resampled and used to evaluate the effect of combining multispectral Pleiades image on the accuracies of segmenting UAV images for tree crown projection area (CPA) estimation and species classification. RGB images from a UAV platform are processed in a photogrametric software and combined with the near-infrared band of a Pleiades image to get a UAV-Pleiades image composite. The images are segmented using the ESP 2 tool and the segmentation accuracy compared using a paired *t*-test. The segmented tree crowns are classified using random trees (RT), support vector machines (SVM), and maximum likelihood (ML) classifiers, and the classification accuracies of the three classifiers are compared using the McNemar's chi-squared test. Our study demonstrates a 93.5% accuracy of segmenting UAV-Pleiades image composite, which is significantly higher than the 84.8% accuracy of segmenting UAV images ($p < 0.05$). Also an 84% classification accuracy of UAV-Pleiades image composite is significantly higher than the 54% classification accuracy of the UAV images ($p < 0.05$). Of the three classifiers used, the classification accuracies of SVM and RT are significantly higher ($p < 0.05$) than that of the ML classifier. Given the significantly high accuracies observed from this study for tree CPA extraction and tree species classification, carbon/above ground biomass modeling is possible with significantly high accuracy using the combination of multispectral Pleiades and UAV images. [DOI: 10.1117/1.JRS.13.034530]

Keywords: unmanned aerial vehicle; multispectral Pleiades; segmentation; tree-species; identification.

Paper 190072 received Jan. 31, 2019; accepted for publication Aug. 29, 2019; published online Sep. 28, 2019.

1 Introduction

Tree species diversity is an important parameter to understand and comprehensively describe a forest ecosystem. Tree species-specific information gives an index of forest biodiversity and ecosystem services, including carbon sequestration. Spatial heterogeneity in species composition and stand structure of forest play a sensitive role in accurate carbon estimation.[1] Forests play a significant role in climate regulation[2] and share 80% of the total exchange of carbon between the atmosphere and the terrestrial ecosystem.[3]

*Address all correspondence to Agbor Esong Effiom, E-mail: agbor29317@alumni.itc.nl

1931-3195/2019/$28.00 © 2019 SPIE

Forest aboveground carbon is about 50% of the above ground biomass (AGB).[4] AGB is the mass of all the organic matter in plant tissues above the soil, including stem, branches, foliage, bark, and seeds.[5] There is a growing need for consistent forest biomass monitoring, in the context of sustainable livelihood, ecosystem services, and reducing emissions from deforestation and forest degradation (REDD+). Under the REDD+ program, member nations must estimate their baseline carbon stocks, monitor, record, and verify any changes due to the implementation of their emission reduction programs to benefit financially.[6,7] To ensure comprehensive and sustainable forest management, carbon assessment methods need to capture tree species-specific information.[8]

Approaches to biomass and carbon estimation include field measurements, GIS-based assessments, and remote sensing.[9] Field assessment for species identification and biomass estimation is too costly and practically impossible. GIS-based methods extrapolate existing forest inventory volume data to biomass using wood density. The extrapolation may induce large errors. Passive remote sensing-based methods rely on the reflectance of the tree crowns recognized from the image and use the statistical relationship between satellite extracted tree parameters [crown projection area (CPA), diameter at breast height (DBH), and tree height (H)] and ground-based measurements for biomass estimation,[5,10,11] using species-specific allometric equations.

The relationship between CPA and DBH for tree species is essential for estimating aboveground carbon. The relationship is built using the CPA extracted from the remotely sensed image. Once the CPA is known, DBH and related biomass can be calculated.[12–15] However, the relation between DBH, CPA, and biomass is species specific, depends on specific wood density, fueling the need to accurately identify tree species within the forest.

High-resolution active sensors such as GeoEye, Worldview, IKONOS, BirdsEye, and Quickbird have been used to identify tree species, extract forest inventory parameters for individual tree species and vegetation classification,[16] and carbon estimation.[17,18] Nevertheless, images from these platforms do not perform well in species identification. Furthermore, temporal availability and continuation of these missions is an issue, creating gaps in forest and carbon monitoring efforts. Also the cost of images from these platforms prohibits communities from reaping the benefits of maintaining their forest under the UN REDD+ program. Multispectral Pleiades data on the other hand are relatively cheaper and readily available with four bands including the near-infrared (NIR) band for differentiating vegetation types. The drawback with Pleiades datasets is that the images lack in spatial resolution for scene description.

Unmanned aerial vehicles (UAVs) are platforms capable of carrying sensors for monitoring and mapping the environment and natural resources. According to Ref. 19, UAVs come with varied capabilities and constitute an essential source of relatively cheaper remote sensing data for applications in many fields, including but not limited to agriculture, forestry, mining, urban planning, and land management. UAVs can be of fixed wing or rotary blade and can carry RGB, multispectral and hyperspectral sensors, or even Lidar depending on the weight of the UAV.[20] Species identification has been carried out using high-resolution optical UAV images.[21,22] The extraction of tree structural parameters[23–26] for carbon estimation has been performed using high-resolution imagery from optical UAV. The results from the mentioned studies have been promising. UAVs capture images with high spatial resolution, and when equipped with multispectral sensors, they provide high spectral resolution images required for segmentation and species identification in the process of object-based image analysis (OBIA). However, multi- or hyperspectral sensors are more expensive than the UAV itself. For this reason, most UAVs use low-cost RGB camera sensors, which produce images with a high spatial but low spectral resolution from which species recognition is challenging.

Accurate species discrimination requires high spectral resolution, whereas a precise description of texture and shape (in segmentation) needs high spatial resolution.[27] However, the inability of a single imaging sensor to completely capture all the necessary information for detecting an object or classify a scene is the reason for the full exploitation of multisource data integration and advanced image analytical or numerical procedures.[27] Image integration is a process of exploiting the strengths of two or more images from the same or different sensors to achieve better results. Most studies involving image integration have done so through one of the many fusion

methods, which end up with spectral and or spatial distortions.[28,29] Image fusion combines and mixes relevant information from a set of images into a single, more informative and complete image.[30] Few studies have simply integrated images by combining or layer stacking relevant bands for segmentation and species identification.

This paper explores the potential of combining a high spatial resolution image from the UAV-RGB platform with the NIR band from relatively inexpensive multispectral Pleiades image for accurate tree crown segmentation and species classification, as a prerequisite for forest carbon estimation.

2 Description of Study Area and Dataset

2.1 *Description of Study Area*

This study was conducted within a nature reserve in Amstelveen village. Amstelveen is a rural area with landscape composed of forest patches and agricultural fields, close to the city of Gronau in Germany. It is at the boundary of the Netherlands and Germany, situated at longitude 32558395m E and 5782262m N of UTM 32 N, ETRS89.

As can be seen in Fig. 1, eight forest blocks can be found in the area, five of which were considered for this study due to the available secondary data on tree species and DBH. The blocks with red polygons were used for this study. The forest blocks have both coniferous and deciduous trees, with different species densities. beech (*Fagus sylvatica*), Scots pine (*Pinus sylvestris*), Oak (*Quercus robur* and *Quercus petraea*), Alder (*Alnus* sp), Douglas fir (*Pseudotsuga menziesii*), European hornbeam, and birch (*Betula* sp) are the most common tree species in the Amstelveen area.[31,32] The tree crowns are at the same canopy level, with spaces in-between. Block 1 is an open forest mainly dominated by Scots pine. Blocks 2–6 are dense mixed forest stands, with tree crowns of different sizes, and at different canopy levels. Each of these blocks consists of more than two tree species.

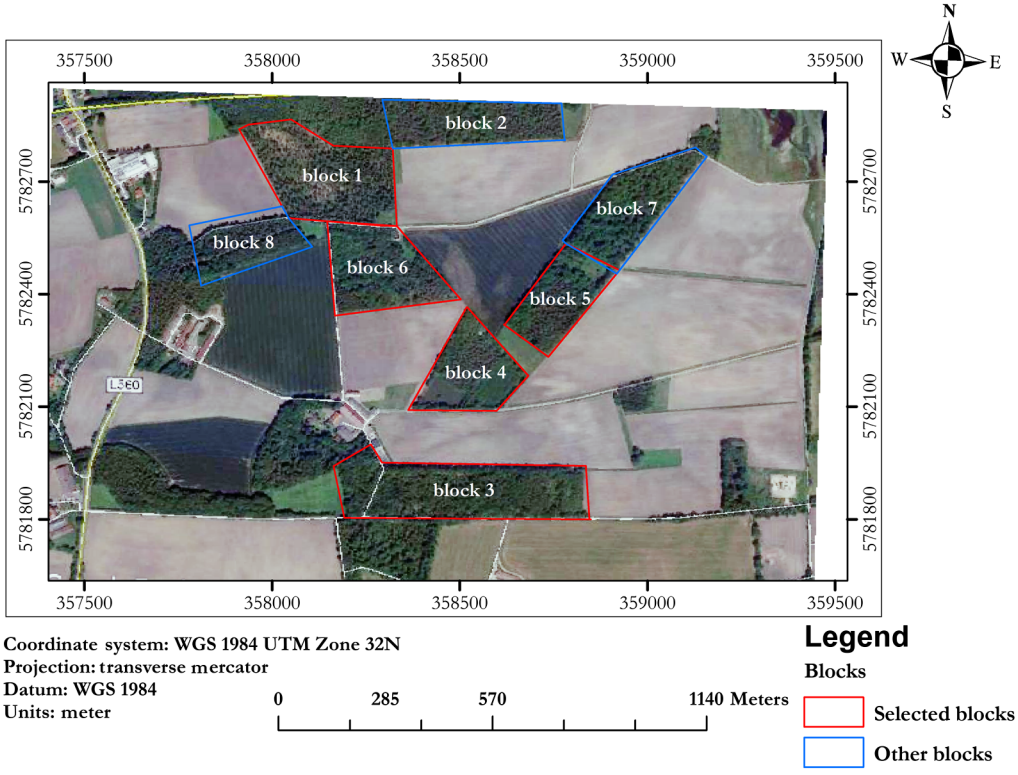

Fig. 1 The study area showing forest blocks selected for this research.

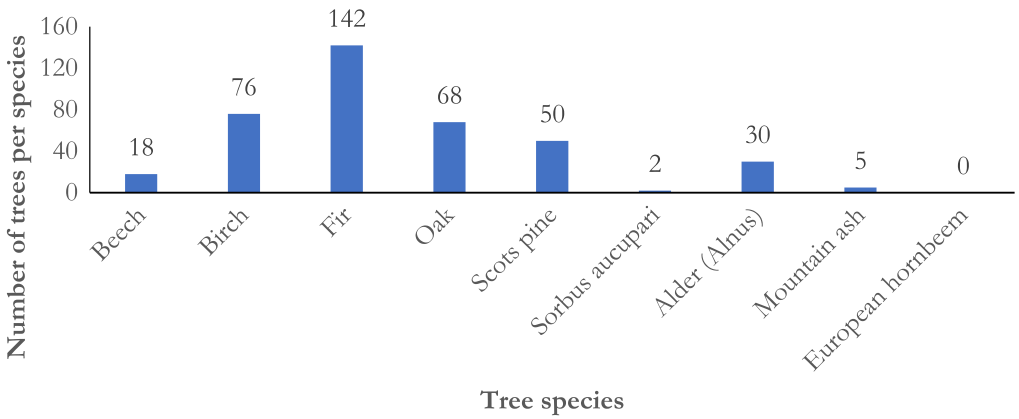

Fig. 2 Numbers of each tree species recorded within the study area.

2.1.1 *Species occurrence*

The bar chart in Fig. 2 shows the occurrence of tree species within the Amstelveen area. From the existing data, a total of 391 trees were extracted. From 391 trees, the dominant species are Fir (36%), birch (19%), Oak (17%), and Scots pine (13%). The other tree species have been recorded in <10% of the samples.

2.2 *Dataset*

This study made use of remotely sensed data from UAV and Pleiades platforms, in combination with field data. UAV images were captured between August and September 2016 at a flight height of 80 m above the tree canopy (100 m above ground), with 80% and 70% forward and side overlap, respectively, using DJ Phantom 4 UAV. Multispectral Pleiades image of the same area with 50-cm resolution captured in September 2014 was sourced from the remote sensing lab in the Faculty of Geo-information Science and Earth Observation (ITC). Field data on tree species, location, and DBH were collected from existing dataset provided by Erdbrügger.[31]

3 Methods

The study had three phases; UAV data acquisition and processing, image segmentation, and classification, as shown in Fig. 3. The methods employed in the different phases of this project are presented in sections following the flow chart.

3.1 *Data Acquisition*

The Pleiades dataset was provided by the ITC. The dataset is orthorectified panchromatic and multispectral (RGB and NIR) images. UAV flights were performed over the 209.2 ha study area after the establishment of eight adequately distributed and appropriately located ground control points (GCPs). The locations of GCPs were measured using the differential Global Navigation Satellite System Leica CS 15, a necessity to optimize the rigidity of the bundle block adjustment (BBA) during image orientation. The flight was conducted with a forward and side overlap of 85% and 70%, respectively. The camera model on board the UAV was GR_GRLENS_18.3_ 4928×3264 (RGB), and the flight height was 80 m above the tree canopy (100 m above the ground). A total of 662 images were collected for processing.

Field data for the same area collected in 2016 were used to continue the study. Data harmonization and extraction made use of GIS operations like query, editing of attribute tables, coordinate reconciliation, overlays, spatial joins, and data export. The extracted point data of tree species and location were overlaid on the orthophoto to confirm with the described fifteen plot locations and tree identities in five of the blocks. According to the lineage of the 2016 data, a

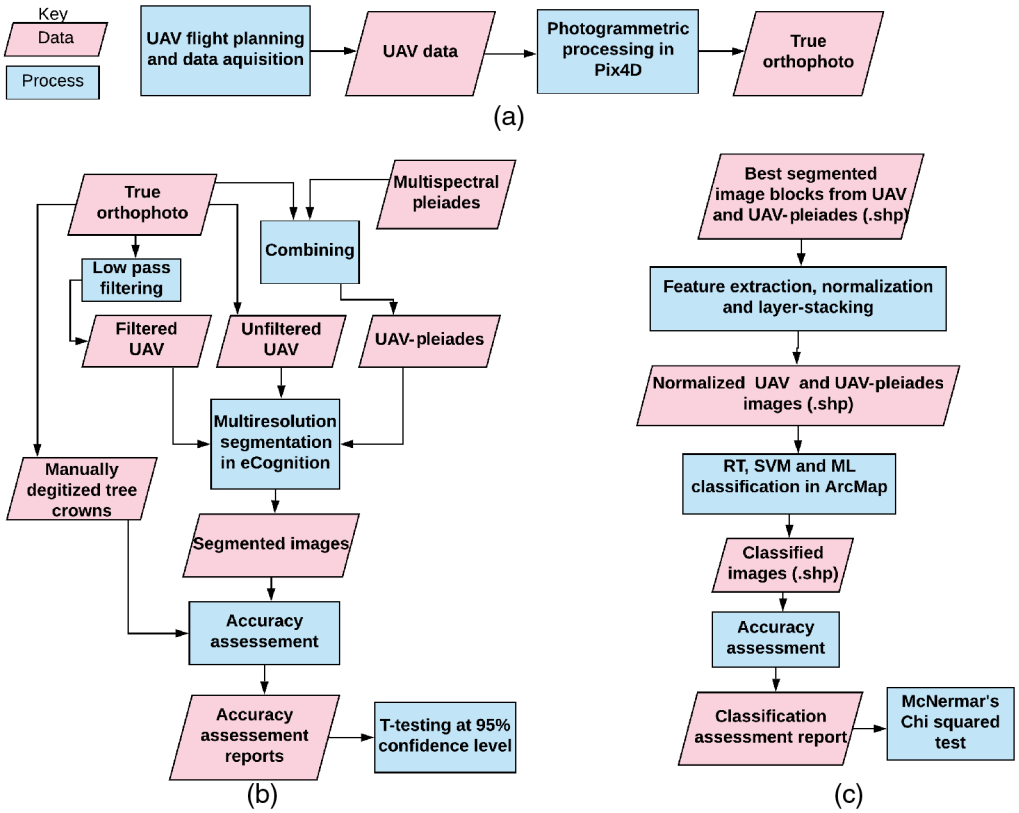

Fig. 3 The different steps involved in the project: (a) UAV data acquisition and processing, (b) segmentation, and (c) classification.

circular plot-based design was used for data collection.[31] All trees with DBH greater than 10 cm were recorded within a 500-m^2 circular plot (12.5-m radius). Tree species, DBH, and location were recorded. Trees with a DBH less than 10 cm were not recorded because their contribution to biomass is assumed to be negligible.[33]

3.2 *Pleiades Data Processing*

The study area was extracted (masked) from the multispectral Pleiades image with a georeferenced shapefile of the study area. The multispectral Pleiades image with the 50-cm resolution was resampled to 30-cm resolution in ArcMap to ensure that pixel corners from UAV and Pleiades coincide. The nearest neighbor resampling algorithm was chosen because it preserves pixel values.[34,35]

3.3 *UAV Data Processing*

The UAV images were processed using structure from motion, the photogrammetric process of constructing the three-dimensional structure of the scene, and camera position by analyzing the sequence of images.[36] The UAV images were processed in Pix4D. Once loaded into the pix4D software, the images go through initial processing, point cloud densification, and finally the generation of digital surface model (DSM) and orthomosaic.

The initial processing begins with tie-point detection, description, and matching for image calibration. A sample of points is iteratively drawn from the pool of matched tie points and used to create a model that determines the best relative orientation of the images. This iterative process called random sample consensus reduces reprojection errors during image orientation.[37] Once the images are sufficiently oriented, GCPs are loaded to optimize the calibration and give the images absolute orientation (geolocation on the ground).

In the second processing phase, the software runs an automatic aerial triangulation with BBA at multiscale mode or half the image size and optimal conditions for point cloud generation and densification.

DSM and orthomosaic were generated in the last processing phase by triangulation, specifying product resolution as default setting (1× ground). Triangulation preserves the characteristics of points from the original image.[38]

The resolution of the UAV orthophoto was high (3.4 cm) and had some noise. It was filtered with a low-pass filter in ArcMap 10.6 and resampled to 30 cm using the nearest neighbor algorithm. Resampling to 30 cm was done because this resolution has been reported to be suitable for segmentation of tree crowns.[32] Filtering removed small objects that induce noise, whereas resampling with the nearest neighbour preserves the spectral information of pixels making up each tree crown and prepares the resolution for better segmentation.

3.4 *Formation of UAV-Pleiades Image Configuration*

UAV-Pleiades image configuration was assembled by layer stacking the red, green, and blue (RGB) bands from the UAV, with the NIR band from the Pleiades image into one raster image using the composite band tool in ArcMap 10.6. This procedure was successful when all the bands to be layer stacked were in the same image depth (8 unsigned or 16 unsigned bits).

3.5 *Image Segmentation*

Segmentation identifies homogenous areas in an image based on shape, colour, size, and groups them into specific objects called segments.[39] There are many different segmentation algorithms, among which multiresolution is powerful when dealing with very high-resolution images.[40] The multiresolution segmentation algorithm was used in this study, and the optimal scale parameter for segmentation was done using the ESP2 tool. This tool automatically segments each image configuration into three levels, corresponding to levels of homogeneity. In this process, the tool calculates local variance of objects for each level (mean standard deviation of objects for each level). The rate of change in local variance per iteration is then plotted against increasing scale value to show the optimum scale value for image segmentation. Figure 4 shows the local variance graph for the segmentation of the open forest block in the study area.

The red line represents the local variation in the image objects from pixel level, whereas the blue line represents the rate of change in local contrast as the object size increases, and the vertical dotted grid lines are the optimal scale for each scene. As can be seen from the graph, the local variance jumps high at the start as the size of objects increases due to the high resolution of the image,[41] whereas the rate of change is in the opposite direction, slowly because of the scene (forest).

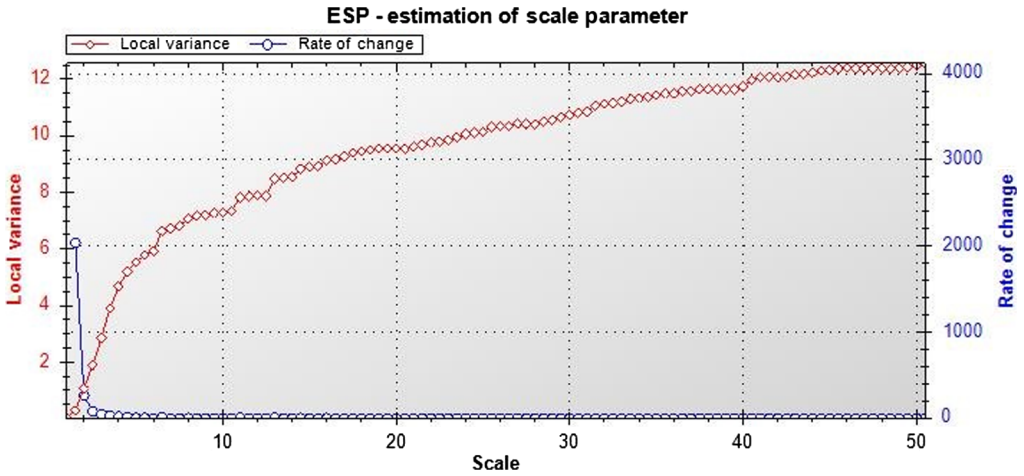

Fig. 4 Local variance, rate of change versus scale parameter for optimal image segmentation using ESP2 tool.

The default parameters (step sizes for each of the three levels, shape, and compactness) in ESP2 tool were inappropriate for segmenting the tree crowns within the forest blocks. In addition to varying the shape and compactness parameters, the step level sizes were iteratively varied to obtain proper segmentation. The best segmentation levels for each forest block were exported as shapefile, smoothed polygon for accuracy assessment in ArcMap.

The entire study area was divided into forest blocks because of differences in forest structure and also to reduce image size for faster processing. The blocks were numbered 1–6. Five of the blocks are those from which field data were collected in 2016, whereas block 2 had no recorded field data.

3.6 *Image Classification*

Object-based supervised image classification is in recent times used for the classification of very high-resolution images.[42,43] Among the most popular classification algorithms for tree species classification are maximum likelihood (ML), random forest, random tree (RT), and support vector machine (SVM) classifiers.[44–46] These classifiers operate using similar principles; use training samples, validation samples, and vote of the plurality to finally classify an object into a specific class.[47] In this study, RT, SVM, and ML classifiers were used and implemented in ArcMap.

The segmented layers were exported from eCognition with five and eight features in the attribute table for UAV and UAV-Pleiades image configurations, respectively. These features represent segment statistics that would be used for classification in ArcMap. The RT, SVM, and ML classifiers in ArcMap require segmented raster as input. For this reason, each feature was extracted by conversion to a segmented raster layer. Features were normalized to avoid attributes with numerically higher ranges from dominating those with numerically lower ranges during classification.[48] Linearizing each feature also avoids numerical difficulties during calculations of segment statistics by the algorithm. Each feature was normalized to have values between 0 and 1, using raster calculator with the expression as follows:

$$\text{normalized feature} = \frac{(\text{feature value} - \text{minimum value})}{(\text{maximum value} - \text{minimum value})}.$$

Normalization also gave each feature the characteristic normal distribution, which makes training and classification faster.[49,50] All normalized features were layer stacked to create a segmented raster layer (a requirement for implementing the classification algorithms in ArcMap) with the number of bands corresponding to the number of features used. Among the layer stacked features, four were selected for classification of UAV (mean values of red, green, blue, and standard deviation), whereas eight were selected for classification of UAV-Pleiades (1, red; 2, green; 3, blue; 4, NIR; 5, mean brightness; 6, compactness; 7, roundness; and 8, standard deviation).

Two sets of training and reference data were digitized in ArcMap based on field data. Training samples were randomly selected, but the digitizing was done such that each sample is a pure representation of the class it represents. Five classes were used: birch, beech, Scots pine, water, and shadow. From the UAV image, 30, 21, 20, 19, and 14 samples of Scots pine, birch, water, beech, and shadow were collected, respectively. On the other hand, 41, 28, 20, 4, and 29 samples of Scots pine, birch, water, beech, and shadow were, respectively, collected from the UAV-Pleiades image. Samples for each class were merged for each image configuration to obtain a value for each class. All classifiers used the same training and validation data set containing five classes (birch, beech, Scots pine, water, and shadow) for the same image configuration. Class separability of the training samples was done using the mean layer statistics. As can be seen in Fig. 5, the plotted ban statistics show that the four classes can be better separated in bands (layers) 1 and 2 for the UAV layer. Within band two, there is a possible mixing of beech and Scots pine.

On the other hand, the four classes are separated within bands 2, 3, 4, and 5 for the UAV-Pleiades image as shown in Fig. 6. In bands 2, 3, and 5, there is a possible mixture of birch and Scots pine, whereas in band 4, all classes are well separated.

With the training data from each image configuration, all three classifiers were trained to generate respective classifier definition files, which were later used for classification. In the case

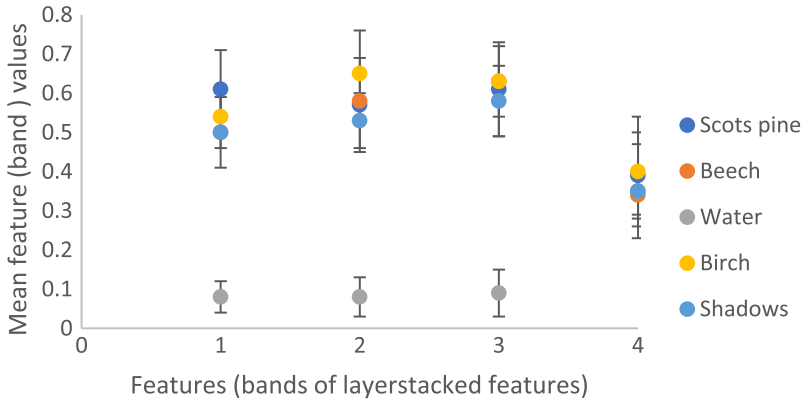

Fig. 5 Comparing class separability among the layers in the UAV layer stack raster (1, red; 2, green; 3, blue; and 4, standard deviation).

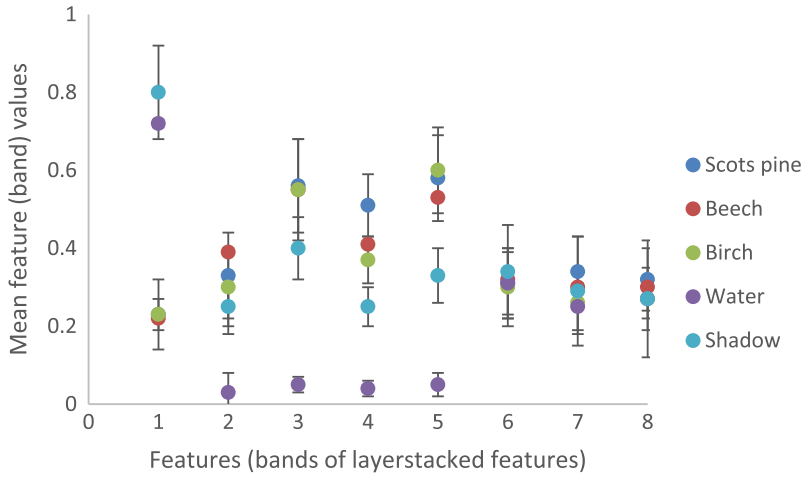

Fig. 6 Comparing class separability between the different image layers (bands) for UAV-Pleiades segmented raster layer. (1, red; 2, green; 3, blue; 4, NIR; 5, mean brightness; 6, compactness; 7, roundness; and 8, standard deviation).

of RT classifier, the number of trees or subset was set to 500 (number of subsets created, classified, and results averaged to get final classification), with a maximum number of samples and sample depth left as default. For SVM, the number of subset per class was set at 500. This number refers to the number of subsets that need to be classified and averaged to get the final classification. These settings were chosen after some iterations.

A vector (shapefile) was created from the classified segments (raster files) and crossed with the segments from eCognition in a spatial joint. The created vector file was the joint feature and the segments from eCognition were target feature. This process created a vector file containing information on class values and species name.

3.7 *Segmentation Accuracy Assessment*

Evaluating the quality of segmentation is essential for the validation of the OBIA process. The best way to measure segmentation accuracy depends on the consequences of any segmentation error. In this study, segmentation is done to estimate tree CPA, an input in species-specific allometric equations for carbon estimation. The consequence of segmentation error is either an overestimation or underestimation of CPA and thus carbon of tree species. For this reason, segmentation accuracy was assessed using area estimation techniques,[39] in a three-step procedure described in Ref. 51, and as shown in the equations as follows:

$$\text{oversegmentation} = 1 - \frac{\text{area}(\text{ADi} \cap \text{ARi})}{\text{area}(\text{ADi})}, \tag{1}$$

$$\text{undersegmentation} = 1 - \frac{\text{area}(\text{ADi} \cap \text{ARi})}{\text{area}(\text{ARi})}, \tag{2}$$

$$\text{total detected error} = \sqrt{\frac{(\text{OS})^2 + (\text{US})^2}{2}}, \tag{3}$$

where ADi is the area of detected objects that are in a one-to-one spatial relationship with reference polygons, ARi is the area of reference polygons, and area (ADi ∩ ARi) is the area of reference polygons that have been correctly segmented.

The accuracy assessment made use of manually digitized polygons obtained for each block from the filtered and resampled orthophoto. 54 polygons were delineated for block 3, 52 for block 5, 123 for block 1, 70 for block 6, and 51 for block 4. A spatial join between reference polygons and the segmented layer was done in ArcMap to identify segmented polygons in a spatial relationship with the reference polygons based on a join count >0. Selection by attribute of polygons from the output based on join count different from zero was made and the results exported as a layer. The reference polygons were used as target features, whereas the segmented layer was joined feature in a spatial join operation. Upon getting the layer of segmented polygons in spatial contact with the reference layer, an intersection was performed with the reference polygon layer to get under segmented and over the segmented area. A field was added to the attribute table of the intersection output and area (ADi ∩ ARi) was obtained by calculating geometry. The area of reference polygon layer represents "ARi" in the equation above, whereas the area of spatial join output represents "ADi." With ADi, ARi, and (ADi ∩ ARi), oversegmentation, under segmentation (US), and total detected error were calculated.

Three blocks were selected to investigate a significant difference in the accuracy of segmenting UAV and UAV-Pleiades image configurations. Using the same reference polygon layer for each block, spatial join, and the intersection was performed with the respective segmented layers. The resulting area from the outputs (intersection) was extracted for corresponding segments and a two-tailed t-test performed at 95% confidence level. For the t-tests to be performed, the extracted data were checked for normality,[52] using skewness and kurtosis z-values. Also the assumption for a homogenous variance was investigated using Levene's F-test.

3.8 *Classification Accuracy Assessment*

Accuracy assessment is a comparison between a detailed map and some reference information assumed to be correct, following acceptable rules consistently.[53] The accuracy of a classification can be judged using accuracy parameters such as overall accuracy (OA), per-class accuracy (CA), producer, and consumer accuracies. The rules to consistently observe in the process include the choice of quality index appropriate given the purpose of each study, sampling unit, strategy, and sample size.[53,54] In this study, the classification was done on a segmented layer with the purpose of accurately linking segments (CPA) to tree species for the modeling of DBH and AGB at the species-specific level. Based on the defined goal, sampling units were chosen as polygons (CPA), and the sample size was proportional. Since the segments (CPA) represents a spatial entity that needs to be given identity in the classification process, the area was chosen as the most important index for accuracy.[55]

Through a spatial query between the segmented layer and the reference polygon layer, a subset of segmented polygons was exported as a test polygon layer. In a spatial join between reference polygons layer and the test polygons layer, class values were transferred from reference to test polygons. A total of 20 samples were taken for Scots pine (692.7 m^2), birch (1604.1 m^2), and water (3087 m^2), whereas 10 and 15 samples were taken for beech (743.5 m^2) and shadow (4103.9 m^2), respectively. An intersection between final test polygons layer and the classified polygons was performed, and the output used to extract correctly and wrongly classified area for each tree species. A selection query by attribute {gridecode = 1 $(2, 3, \ldots n)$ AND class = 1 $(2, 3, \ldots n)$} was performed, and the area of each species correctly and wrongly classified was

calculated. The values were input into the confusion matrix for classification accuracy assessment.

A selection by location query was performed between a reference layer and each of the classified layers to extract samples from each layer for comparison. A spatial joint was done with the three layers, reference, and exported test segments from each classified layer. The class values from corresponding segments in both classified layers were judged against those from the reference layer, and a 2×2 confusion matrix was created. A statistical test was performed to infer a significant difference in the classification of different classifiers using the McNemar test as described in Ref. 56. This test is based on chi-square (z^2) statistics computed from the two error matrices given as

$$Z^2 = (f_{12} - f_{21})^2/(f_{12} + f_{21}),$$

where f_{12} is the number of cases wrongly classified by classifier one but correctly classified by classifier 2, and f_{21} is the number of cases correctly classified by classifier one but wrongly classified by classifier 2. From the McNemar test, if the z-score is >1.96 at 95% confidence level, then the differences in classification results are statistically significant.

4 Results

4.1 *Effect of Adding Multispectral Pleiades Image on Tree Crown Segmentation Accuracy of UAV*

As shown in Fig. 7, the segmentation results of blocks 6 (dense mixed forest with large tree crowns) and 5 (dense mixed forest with closed canopy) show some cases of over and US. However, a quantitative assessment is presented below.

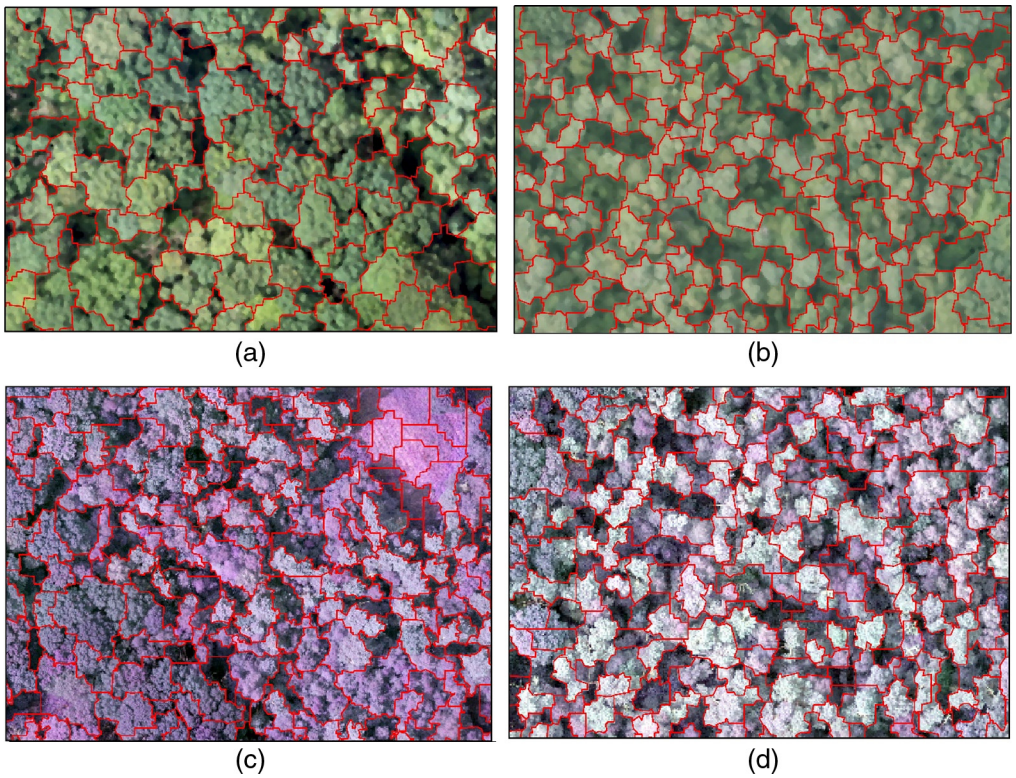

Fig. 7 Visual comparison of UAV (a and b) and UAV-Pleiades (c and d) segmentation using blocks 6 and 5 (a and c) are block 6 UAV and UAV-Pleiades, respectively, while b and d are block 5 (UAV and UAV-Pleiades, respectively).

Table 1 Segmentation accuracy of UAV and UAV-Pleiades images using five forest blocks (OS, oversegmentation; US, undersegmentation; and TDE, total detected error).

	Block 1	Block 3	Block 4	Block 5	Block 6
UAV					
OS	0.22	−0.01	0.31	−0.21	−0.27
US	0.00	0.25	0.00	0.00	0.00
TDE	0.16	0.18	0.22	0.15	0.19
Accuracy	84.36	81.97	78.20	84.80	80.94
UAV-Pleiades					
OS	0.51	0.38	−0.11	−0.09	0.10
US	0.00	0.00	0.00	0.02	0.00
TDE	0.36	0.27	0.08	0.06	0.07
Accuracy	64.18	73.15	91.87	93.50	92.70

Table 2 Normality test using skewness z value for data meant for assessing the effect of image configuration on area segmented for forest blocks 1, 3, 4, and 6. (UAV-PI, UAV-Pleiades; Skew-z and Kur-z are skewness and Kurtosis z-value, respectively; and SE, error).

	UAV block 1	UAV block 3	UAV block 4	UAV block 6	UAV-PI block 1	UAV-PI block 3	UAV-PI block 4	UAV-PI block 6
Mean	30.42	60.25	51.23	81.31	47.54	108.59	54.34	91.40
S.E	0.84	2.80	2.57	3.14	1.55	7.02	3.14	4.13
Kurtosis	2.70	5.68	3.87	3.89	4.08	16.69	7.33	9.54
Skewness	1.36	1.98	1.82	1.67	1.60	3.44	2.12	2.33
Count	486	252	170	296	378	176	168	275
Skew-z	0.61	1.41	1.41	1.88	0.97	**2.04**	1.48	1.77
Kur-z	0.31	0.49	0.67	0.81	0.38	0.42	0.43	0.43

Note: The number 2.04 is in bold to indicate that the areas from segments of UAV-Pleiades block 3 are not sufficiently normally distributed since skewness z-value is >1.98. As explained in the text that a log transformation made it sufficiently normally distributed, satisfying the condition to perform a t-test.

As can be seen in Table 1, the UAV-Pleiades image shows highest segmentation accuracy in block 5 (93.5%) and lowest in block 1 (64.2%), compared to the UAV with 84.8% and 84.4% in blocks 5 and 1, respectively. The addition of Pleiades image seems to have enhanced segmentation accuracy in the case of blocks 4, 6, and 5.

To test the hypothesis of no significant difference in the mean area segmented from UAV and UAV-Pleiades image configurations, a student t-test was performed. As can be seen in Table 2, the distributions of the data extracted from best segmentation of the image categories are sufficiently normal to conduct a student t-test,[52] except in the case of the UAV-Pleiades segments for block 3. However, a log transformation of the UAV-Pleiades block 3 data made it significantly normally distributed (skewness = 0.07, $<|2.0|$). Their skewness z-value ($<|2.0|$) and kurtosis z-value ($<|9.0|$) of the other blocks are within acceptable range.

Also Levene's F-test was done to test the assumption of homogeneous variance. As can be seen in Table 3, $F(11) = 65.91$, $p = 9.2 \times 10^{-135}$, there is a significant difference in the variances at 95% confidence level. Thus the null hypothesis of equal variances was rejected, and an independent t-test with unequal variances was performed.

Table 3 ANOVA results of Levene's test for the theory that segmented area from the different image configurations has equal variances.

Source of Var.	SS	df	MS	F	p-value	F crit.
Between groups	696807.7	11	63346.15	65.91	9.2×10^{-135}	1.79
Within groups	3,477,524	3618	961.17			
Total	4,174,331	3629				

Table 4 Independent t-test results for the hypothesis that there is no significant difference in the area segmented for UAV and UAV-Pleiades images at 95% confidence level.

	Block 1 $n_f = 486$ $n_{pl} = 378$ H_0, $\mu_1 = \mu_2$ $d_f = 589$	Log (block 3) $n_f = 252$ $n_{pl} = 176$ H_0, $\mu_1 = \mu_2$ $d_f = 379$	Block 4 $n_f = 170$ $n_{pl} = 168$ H_0, $\mu_1 = \mu_2$ $d_f = 323$	Block 6 $n_f = 296$ $n_{pl} = 275$ H_0, $\mu_1 = \mu_2$, $d_f = 521$
t stat	−9.70	−8.60	−0.77	1.95
$P(T \leq t)$ 1-tail	4.93×10^{-21}	1.05×10^{-16}	2.22×10^{-01}	2.60×10^{-02}
t-crit., 1-tail	1.65	1.65	1.65	1.65
$P(T \leq t)$, 2-tail	9.86×10^{-21}	2.11×10^{-16}	4.44×10^{-01}	5.20×10^{-02}
t-crit., 2-tail	1.96	1.97	1.97	1.96
	Significant	Significant	Not significant	Significant (1-tail)

n_f, sample size for filtered UAV image; n_{pl}, sample size for UAV-Pleiades image; and H_0, null hypothesis.

In the case of UAV and UAV-Pleiades, as can be seen in Table 4, the one tail t-test with unequal variance is associated with a significant difference between blocks 1 ($p = 4.93 \times 10^{-21}$), 6 ($p = 2.60 \times 10^{-02}$), and 3 ($p = 1.05 \times 10^{-16}$). Block 4 did not show any significant difference ($p = 2.22 \times 10^{-01}$) in the area segmented for both image configurations.

4.2 *Classification of UAV and UAV-Pleiades Image Configurations*

The classification of UAV and UAV-Pleiades images was performed using ML, RT, and SVM classifiers in ArcMap. The classification accuracies were compared between the two image configurations and across the three classifiers. The results presented in the subsequent sections.

4.3 *Classification of UAV Images (Area-Based)*

The detailed maps of ML, RT, and SVM classifications for forest block 4 are presented in Fig. 8. From the maps, it can be deduced that the identification of tree species (beech, birch, and Scots pine), and their surrounding environment from the UAV image configuration yielded good results using the three classifiers. The RT classification produced a higher OA of 62%, compared to 60.6% and 51.7% for SVM and ML classifiers, respectively. Errors could, however, be visually recognized between the water and shadow classes.

As can be seen in Fig. 9, the classification of Scot pine is 44.7%, 39.3%, and 49.3% for SVM, RT, and ML classifiers, respectively. 24.2% of beech was correctly classified by SVM and RT, whereas ML classifier correctly classified 18.2%. All three classifiers registered an accuracy >40% for classification of birch species. Greater than 50% of the classifications of SVM and RT are in better agreement (kappa of 53.5% and 53.7%, respectively), whereas <50% of the classification of ML is in better agreement (kappa of 45.7%).

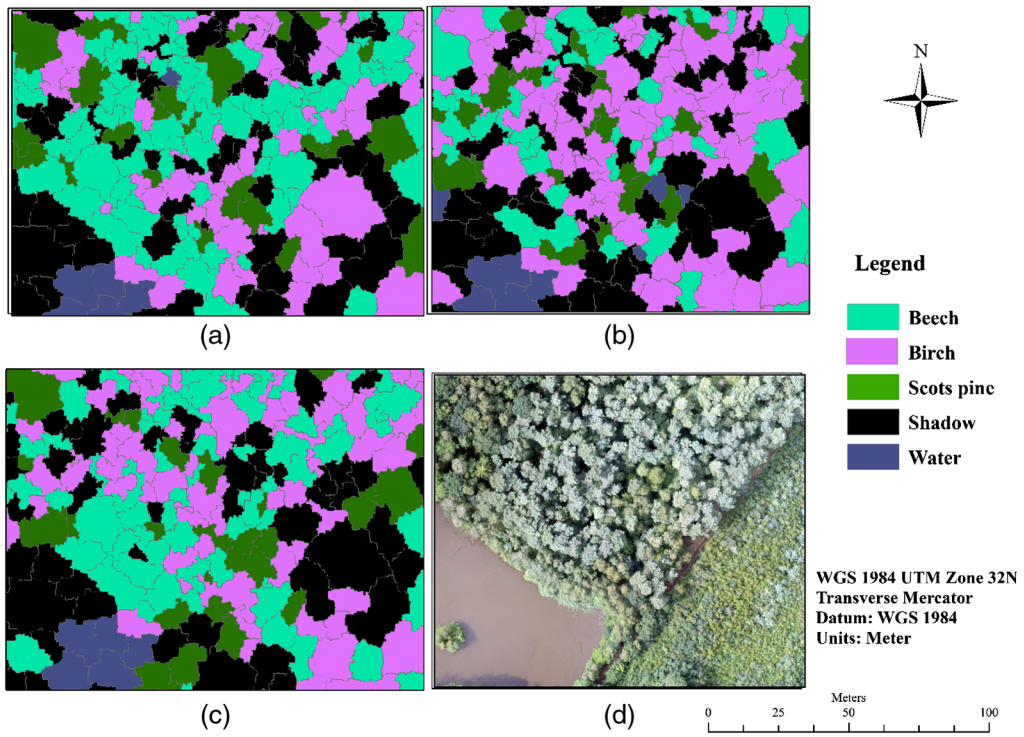

Fig. 8 (a) ML, (b) RT, (c) SVM, and (d) classification of UAV image of block 4 in ArcMap.

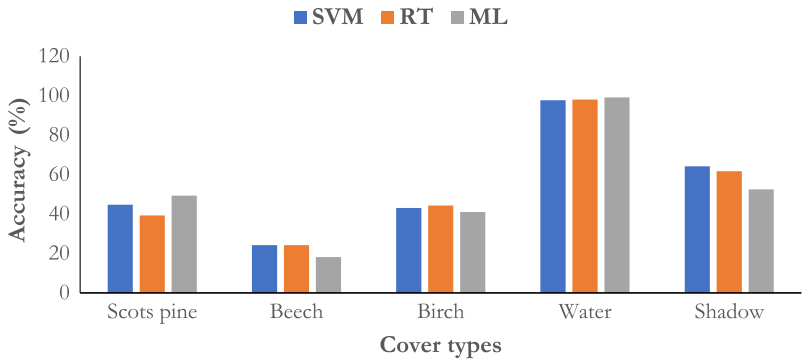

Fig. 9 CA for the classification of Scots pine ($n = 20$), beech ($n = 10$), birch,[20] and their environment (water and shadow) using SVM, RT, and ML classifiers.

4.4 *Classification of UAV-Pleiades Image Using Three Classifiers*

The tree species maps from ML, RT, and SVM classifications for block 4 are presented in Fig. 10. From the maps, it is clear that using the three classifiers, the discrimination of tree species (beech, birch, and Scots pine) and their surrounding environment yielded good results from the UAV-Pleiades image configuration. The SVM and RT classification produced a higher OA of 84%, compared to the 74.8% for ML classifiers, respectively.

The classification results were best in identifying Scots pine and birch using all three methods as shown in Fig. 11. Among the tree species, beech had the lowest classification accuracy for all classifiers.

A comparison of CA reveals a general increase in the class accuracies recorded for UAV-Pleiades image compared to the UAV image as shown in Fig. 12.

The addition of Pleiades to UAV image increased the classification accuracy when using all three of the classification algorithms. The classification accuracy of UAV-Pleiades image configuration is higher when using SVM and RT, compared to the ML classifier.

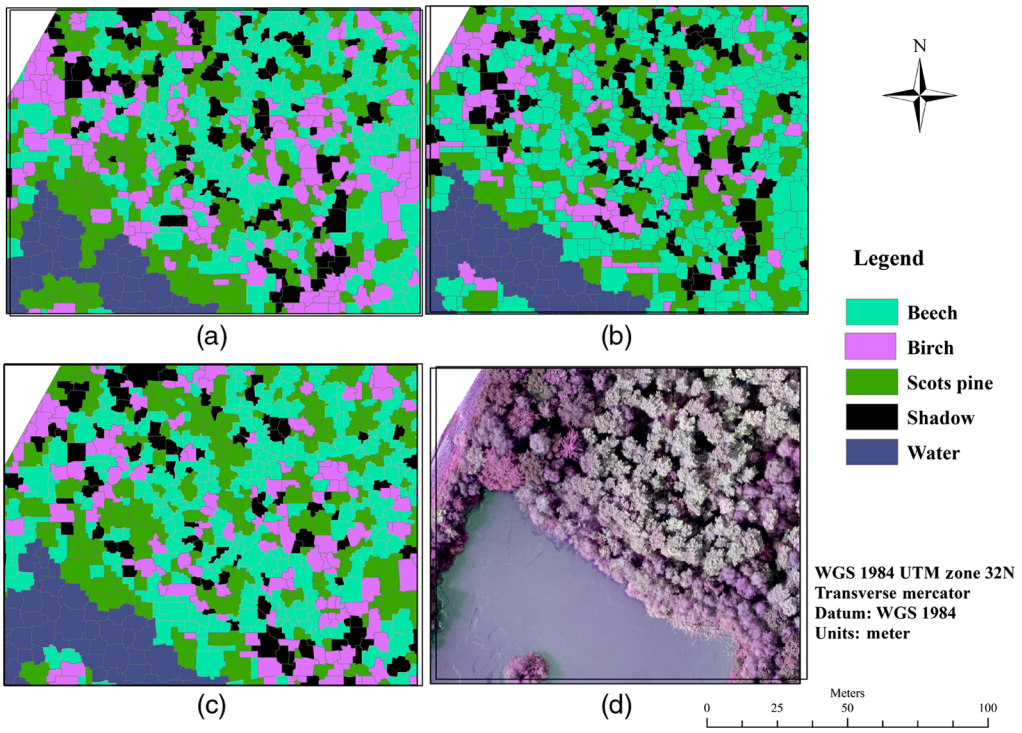

Fig. 10 (a) ML, (b) RT, (c) SVM, and (d) classifications of UAV-Pleiades block 4 in ArcMap.

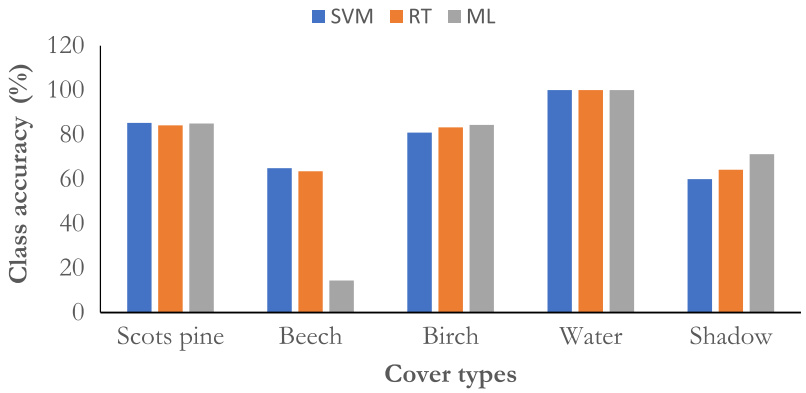

Fig. 11 Class accuracies for each cover type using SVM, RT, and ML classification algorithm.

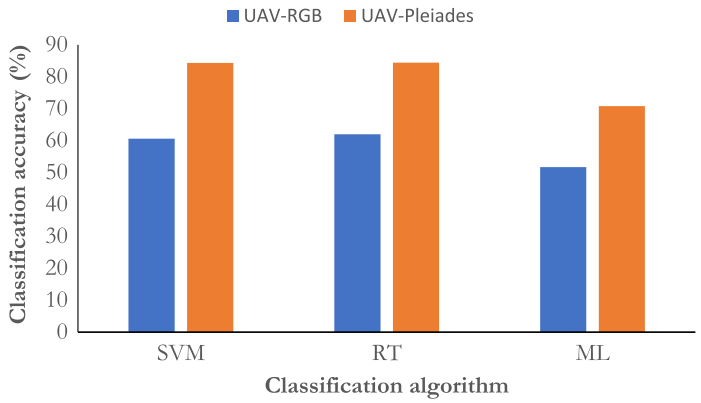

Fig. 12 Comparing the classification accuracy of UAV and UAV-Pleiades image configurations using ML, RT, and support.

Table 5 Comparison of the classification accuracies (%) of tree species and their environment for two image configurations and three classifiers.

	UAV							UAV-Pleiades						
	Sp	Bi	Be	Wa	Sh	OA	Kappa	Sp	Bi	Be	Wa	Sh	OA	Kappa
SVM	44.7	43.1	24	97.7	61.7	62	0.54	84.2	83.3	63.5	100	64.2	84.3	0.8
RT	39.3	44.3	24	98	61.7	62	0.54	85.3	81	65	100	63.4	84.4	0.8
ML	49.3	41	18	99.1	52.5	51.7	0.46	85	84.4	14.3	100	71.2	70.8	0.62

Sp, Scots pine; Bi, birch; Be, beech; Wa, water; Sh, shadow; OA, overall accuracy; RT, random trees; SVM, support vector machines; and ML, maximum likelihood.

Table 6 Comparison between SVM, RT, and ML classifiers using McNemar's chi-squared statistic.

	SVM versus RT	SVM versus ML	RT versus ML
McNemar's chi-squared statistic	0.6	2.8	2.5

4.4.1 *Classification accuracy assessment*

The confusion matrix derived from the classification of both image configurations by the three classifiers is presented in Table 5. The matrices consist of OA, the degree of agreement between the detailed image and reality (kappa value), and CA. The kappa value, OA, and CA for UAV-Pleiades image configuration are higher compared to that from the UAV image. The three classifiers could identify Scots pine (Sp) and birch (Bi) from the UAV-Pleiades image with an accuracy of >80%. RT and SVM classifiers were able to discriminate beech (Be) and birch (Bi) species from UAV-Pleiades image with an accuracy (CA) of >60%, compared to the 14% accuracy recorded by ML classifier for the same UAV-Pleiades image configuration.

The UAV-Pleiades classifications were used to investigate significant differences in the performance of the three classifiers using the McNemar test. The results are presented below.

4.5 *Comparing SVM, RT, and ML Classification Results*

From the classified segments, a total of 113 test segments were extracted using the reference polygons. The McNemar's test[44] investigates if the difference in the number of misclassified test polygons is significant. As can be seen in Table 6, the McNemar's chi-squared statistic between SVM and RT classifiers is <1.98 at the 95% confidence level. If the test statistic is <1.98, any difference is not significant.[56] The differences in these classifications were found not significant. In the case of SVM and ML and between RT and ML classifiers, the McNemar's chi-squared statistic is >1.98. There is a significant difference in the classification of SVM and ML and between RT and ML.

5 Discussion

5.1 *Segmentation of UAV and UAV-Pleiades Image Blocks*

The segmentation accuracy of the UAV-Pleiades image blocks was higher than the accuracy of segmenting UAV image blocks. The higher segmentation accuracy of UAV Pleiades image suggests that the addition of Pleiades NIR band to UAV enhanced the segmentation accuracy. The enhancement was statistically significant in blocks 1, 6, and 3. The significant improvement could be likened to the spatial arrangement and vertical structure of tree species within each of these blocks. Block 1 is an open forest with mostly Scots pine, with visible crowns that are

closed within the same canopy. Addition of the NIR band from the Pleiades must have reduced the effect of shadow that exists in the UAV image, increased spectral variation, clearly showing boundaries that resulted in better segmentation accuracy.[57] Block 6 is composed of Scots pine, oak, birch, and beech, with each species grouped within the same canopy level. Block 3 has the birch and Scots pine occupying specific locations and also within the same canopy level. This spatial arrangement of tree species in these blocks, with each species occupying a particular vertical space, might have contributed to the high segmentation accuracy. Also the addition of the NIR band from the Pleiades must have increase spectral variations between the crowns of tree species in these blocks and so enhance segmentation. The segmentation accuracy associated with the addition of Pleiades to UAV is higher than the results of segmenting high-resolution images such as Geo-eye and worldview.[58,59] The differences in results might be partly because of the ESP2 tool, which was not used in the cited cases.

5.2 *Classification of UAV and UAV-Pleiades Image Blocks*

The classification of different tree species in a mixed forest can be challenging using high-resolution UAV or the multispectral Pleiades as standalone. The class accuracies for UAV image block range from 49.3% in Scots pine to 24% in beech species for all three classifiers. The low accuracy of classifying beech species is probably because of fewer samples of beech and high spectral mixing between beech and Scots pine. Also the beech trees were younger, so they mostly occupied the lower canopy and its crowns were shaded by the shadows of mature and taller trees, causing it to be seen and classified as a shadow. The observed high accuracy in the case of UAV-Pleiades image configuration can be explained by the sensitivity of the NIR band from the Pleiades to species. The OA and kappa value recorded in this study for the three classifiers are higher than that discussed in some works.[44,56] The higher accuracy could be due to the high spatial resolution of images used in this study compared to the 5-m resolution of RapidEye dataset used in the other studies. High spatial resolution images display more features and allow the features to be differentiated, compared to lower or coarse resolution images, thus resulting in higher classification accuracies.[60–62] The classification procedure and environment may also have had an influence. The present study performed classification in ArcMap, whereas the cited case classified in MATLAB. This study made use of a feature normalization method as described in Hsu et al.[48] According to Ref. 49, different normalization methods may exert different effects on different classifiers. However, the impact of feature normalization methods on classifiers was not assessed in this work.

The McNemar test z-score <1.96 for SVM and RT, mean that there is no significant difference between the classifiers. However, the classifications of ML and SVM, and ML and RT are significantly different at the 95% confidence level (test statistic >1.96). SVM and RT performed significantly better than the ML. This result is in line with other works,[44,56,63] stating that RT and SVM are much better classifiers for tree species identification compared to ML. The reason might be because SVM and RT classifiers perform multiple classifications of each object as specified by the user, then perform a vote of the plurality to get the best classification for each object. The iterative process minimizes chances of misclassification. Also these two classifiers require a limited number of pure samples to get a reasonable classification.

6 Conclusions and Recommendations

This study has demonstrated the utility of combining the flexible UAV and multispectral Pleiades images for tree CPA estimation and tree species identification. The findings assert with existing literature that image integration has potential to enhance the accuracies of segmenting tree crowns and classifying tree species with higher accuracies, sufficiently significant for accurate forest carbon modeling. The procedures employed in this research are simple and easily reproduceable as requested by the REDD+ program. The specific conclusions from this study are highlighted below.

1. The combination of UAV and multispectral Pleiades image (50 cm) can be used for tree crown segmentation and tree species classification in view for carbon estimation.

2. The addition of the NIR band from multispectral Pleiades image significantly enhanced the accuracy of segmenting tree crowns from UAV image with 95% confidence.
3. The addition of the NIR band from multispectral Pleiades image significantly enhanced the accuracy of classifying tree species from UAV image with 95% confidence.
4. Given the significantly high segmentation and classification accuracies, the addition of multispectral Pleiades image (50 cm) to the UAV image for accurate modeling of carbon and aboveground biomass would yield reliable results.

The use of a canopy height model could increase the accuracy of segmenting low- and high-level trees, resulting in more accurate tree crown estimation. Thus this study recommends the use of the NIR and RGB bands as separate layers with weights in eCognition and the inclusion of canopy height model for segmentation.

Acknowledgments

The authors would like to thank the Faculty of ITC, the University of Twente for providing the finance through ITC-UTS scholarship, space, equipment, and software to conduct this research.

References

1. Y. Hu et al., "Influence of tree species composition and community structure on carbon density in a subtropical forest," *PLoS One* **10**(8), e0136984 (2015).
2. FAO, *Global Forest Resources Assessment 2010*, 163rd ed., Vol. **163**, FAO Forestry Paper, FAO, Rome (2010).
3. U. Koju, J. Zhang, and H. Gilani, "Exploring multi-scale forest above ground biomass estimation with optical remote sensing imageries," *IOP Conf. Ser. Earth Environ. Sci.* **57**(1), 012011 (2017).
4. G. Assefa et al., "Training manual ON: forest carbon pools and carbon stock assessment in the context of SFM and REDD+," p. 74 (2013).
5. H. K. Gibbs and M. Herold, "Tropical deforestation and greenhouse gas emissions," *Environ. Res. Lett.* **2**(4), 045021 (2007).
6. G. Patenaude, R. Milne, and T. P. Dawson, "Synthesis of remote sensing approaches for forest carbon estimation: reporting to the Kyoto Protocol," *Environ. Sci. Policy* **8**, 161–178 (2005).
7. B. S. Ward, "The global forest observations initiative (GFOI)," (2013).
8. W. S. Schwenk et al., "Carbon storage, timber production, and biodiversity: comparing ecosystem services with multi-criteria decision analysis," *Ecol. Appl.* **22**(5), 1612–1627 (2012).
9. D. Lu, "The potential and challenge of remote sensing-based biomass estimation," *Int. J. Remote Sens.* **27**(7), 1297–1328 (2006).
10. Z. Zhang, L. Cao, and G. She, "Estimating forest structural parameters using canopy metrics derived from airborne LiDAR data in subtropical forests," *Remote Sens.* **9**(9), 940 (2017).
11. J. C. White et al., "Remote sensing technologies for enhancing forest inventories: a review," *Can. J. Remote Sens.* **42**, 619–641 (2016).
12. M. H. Obeyed, "Predictive models between diameter, height, crown diameter and age of Pinus brutia ten. in Zawita and Atrush districts," *Glob. J. Bio-Sci. Biotechnol.* **3**(2), 203–210 (2014).
13. Q. Onilude et al., "Modelling DBH and crown diameter for Triplochiton scleroxylon (K. Schum) in Nigeria," *Acad. J. Sci. Res.* **3**(11), 178–83 (2015).
14. S. K. Shah and H. Acharya, "Modelling the relationship between canopy projection area and above-ground carbon stock of intermingled canopy trees using high-resolution satellite imagery," *Banko Janakari.* **23**(2), 20–29 (2016).
15. R. P. Sharma, Z. Vacek, and S. Vacek, "Individual tree crown width models for Norway spruce and European beech in Czech Republic," *For. Ecol. Manage.* **366**, 208–220 (2016).
16. M. A. Wulder et al., "Comparison of airborne and satellite high spatial resolution data for the identification of individual trees with local maxima filtering," *Int. J. Remote Sens.* **25**(11), 2225–2232 (2004).

17. Y. K. Karna et al., "Integration of WorldView-2 and airborne LiDAR data for tree species level carbon stock mapping in Kayar Khola watershed, Nepal," *Int. J. Appl. Earth Obs. Geoinf.* **38**, 280–291 (2015).
18. F. E. Fassnacht et al., "Review of studies on tree species classification from remotely sensed data," *Remote Sens. Environ.* **186**, 64–87 (2016).
19. F. Nex and F. Remondino, "UAV for 3D mapping applications: a review," *Appl. Geomatics* **6**, 1–15 (2014).
20. W. M. Bailey, "Unmanned aerial vehicle path planning and image processing for orthoimagery and digital surface model generation," Master's Thesis, Vanderbilt University, University of Vanderbilt, Nashville (2012).
21. R. Näsi et al., "UAS based tree species identification using the novel FPI based hyperspectral cameras in visible, NIR and SWIR spectral ranges," *ISPRS Int. Arch. Photogramm. Remote Sens. Spat. Inf. Sci.* **XLI-B1**, 1143–1148 (2016).
22. O. Nevalainen et al., "Individual tree detection and classification with UAV-based photogrammetric point clouds and hyperspectral imaging," *Remote Sens.* **9**(3), 185 (2017).
23. A. C. Birdal, U. Avdan, and T. Turk, "Estimating tree heights with images from an unmanned aerial vehicle," *Geomatics Nat. Hazards Risk* **5705**, 1–13 (2017).
24. A. D.-V. Ramon et al., "High-resolution airborne UAV imagery to assess olive tree crown parameters using 3D photo reconstruction: application in breeding trials," *Remote Sens.* **7**(4), 4213–4232 (2015).
25. P. J. Zarco-Tejada et al., "Tree height quantification using very high resolution imagery acquired from an unmanned aerial vehicle (UAV) and automatic 3D photo-reconstruction methods," *Eur. J. Agron.* **55**, 89–99 (2014).
26. N. Ye, L. Van Leeuwen, and P. Nyktas, "Analysing the potential of UAV point cloud as input in quantitative structure modelling for assessment of woody biomass of single trees," *Int. J. Appl. Earth Obs. Geoinf.* **81**, 47–57 (2019).
27. H. Ghassemian, "A review of remote sensing image fusion methods," *Inf. Fusion* **32**, 75–89 (2016).
28. V. R. Pandit and R. J. Bhiwani, "Image fusion in remote sensing applications: a review," *Int. J. Comput. Appl.* **120**(10), 22–32 (2015).
29. R. Sivagami et al., "Review of image fusion techniques and evaluation metrics for remote sensing applications," *Indian J. Sci. Technol.* **8**(35) (2015).
30. D. K. Sahu and M. P. Parsai, "Different image fusion techniques—a critical review," *Int. J. Mod. Eng. Res.* **2**(5), 4298–4301 (2012).
31. J. Erdbrugger, "Comparing tree parameters extracted from UAV images and TLS data sets comparing tree parameters extracted from UAV images and TLS data sets," Master's Thesis, Faculty of Geo-Information Science and Earth Observation (ITC), University of Twente, Netherlands (2017).
32. J. A. Okojie, "Assessment of forest tree structural parameter extractability from optical imaging UAV datasets, in Ahaus Germany," Master's Thesis, Geo-Information Science and Earth Observation (ITC), University of Twente, Netherlands (2017).
33. S. Brown, "Measuring carbon in forests: current status and future challenges," *Environ. Pollut.* **116**, 363–372 (2002).
34. W. Bakx et al., "Pre-processing," in *The Core of GISience: A Processed-Based Approach*, V. Tolpekin and A. Stein, Eds., 2013th ed., p. 524, Faculty of Geo-Information Science and Earth Observation (ITC), University of Twente, Enschede (2013).
35. D. S. S. Baboo and M. R. Devi, "An analysis of different resampling methods in Coimbatore, district," *Global J. Comput. Sci. Technol.* **10**(15), 61–6 (2010).
36. P. F. Alcantarilla, A. Bartoli, and A. J. Davison, "KAZE features," *Lect. Notes Comput. Sci.* **7577**, 214–227 (2012).
37. M. A. Fischler and R. C. Bolles, "Random sample consensus: a paradigm for model fitting with applications to image analysis and automated cartography," *Commun. ACM* **24**(6), 381–395 (1981).
38. Pix4D SA, *Pix4Dmapper 4.1 Use Manual*, 2017th ed., Pix4D SA, Ed., p. 305, Pix4D, Lausanne (2017).

39. M. Möller, L. Lymburner, and M. Volk, "The comparison index: a tool for assessing the accuracy of image segmentation," *Int. J. Appl. Earth Obs. Geoinf.* **9**(3), 311–321 (2007).
40. M. Belgiu and L. Dragut, "Comparing supervised and unsupervised multiresolution segmentation approaches for extracting buildings from very high resolution imagery," *ISPRS J. Photogramm. Remote Sens.* **96**, 67–75 (2014).
41. L. Draguţ, D. Tiede, and S. R. Levick, "ESP: a tool to estimate scale parameter for multiresolution image segmentation of remotely sensed data," *Int. J. Geogr. Inf. Sci.* **24**(6), 859–871 (2010).
42. R. C. Weih and N. D. Riggan, "Object-based classification vs. pixel-based classification: comparative importance of multi-resolution imagery," *Int. Arch. Photogramm. Remote Sens. Spat. Inf. Sci.* **XXXVIII**, 1–6 (2010).
43. E. Juniati and E. N. Arrofiqoh, "Comparison of pixel-based and object-based classification using parameters and non-parameters approach for the pattern consistency of multi scale landcover," *Int. Arch. Photogramm. Remote Sens. Spat. Inf. Sci.* **XLII-2/W7**, 765–771 (2017).
44. S. Adelabu et al., "Exploiting machine learning algorithms for tree species classification in a semiarid woodland using RapidEye image," *J. Appl. Remote Sens.* **7**(1), 073480 (2013).
45. M. A. Cho et al., "Improving discrimination of Savanna tree species through a multiple-endmember spectral angle mapper approach: canopy-level analysis," *IEEE Trans. Geosci. Remote Sens.* **48**(11), 4133–4142 (2010).
46. A. Carleer and E. Wolff, "Exploitation of very high resolution satellite data for tree species identification," *Photogramm. Eng. Remote Sens.* **70**(1), 135–140 (2004).
47. *eCognition® Developer*, 2016th ed., pp. 1–267, Trimble Germany GmbH, Munich, Germany (2016), www.eCognition.com.
48. C. Hsu, C. Chang, and C. Lin, "A practical guide to support vector classification," 2010, http://citeseerx.ist.psu.edu/viewdoc/summary?doi=10.1.1.224.4115 (accessed 31 July 2017).
49. A. Kuzmin et al., "Automatic segment-level tree species recognition using high resolution aerial winter imagery," *Eur. J. Remote Sens.* **49**(1), 239–259 (2016).
50. J. Hua et al., "Normalization benefits microarray-based classification," *EURASIP J. Bioinf. Syst. Biol.* **2006**, 043056 (2006).
51. N. Clinton et al., "An accuracy assessment measure for object based image segmentation," *Photogramm. Eng. Remote Sens.* **76**, 289–299 (2010).
52. E. Schmider et al., "Is it really robust?" *Methodology* **6**(4), 147–151 (2010).
53. A. H. Strahler et al., "Global land cover validation: recommendations for evaluation and accuracy assessment of global land cover maps," Vol. **48**, Italy (2006).
54. D. Lu and Q. Weng, "A survey of image classification methods and techniques for improving classification performance," *Int. J. Remote Sens.* **28**(5), 823–870 (2007).
55. J. Radoux and P. Bogaert, "Good practices for object-based accuracy assessment," *Remote Sens.* **9**(7), 646 (2017).
56. R. Manandhar, I. O. A. Odeh, and T. Ancev, "Improving the accuracy of land use and land cover classification of Landsat data using post-classification enhancement," *Remote Sens.* **1**(3), 330–344 (2009).
57. R. Pu and S. Landry, "A comparative analysis of high spatial resolution IKONOS and WorldView-2 imagery for mapping urban tree species," *Remote Sens. Environ.* **124**, 516–533 (2012).
58. S. Baral, "Mapping carbon stock using high resolution satellite images in sub-tropical forest of Nepal," Master's Thesis, University of Twente Faculty, Geo-Information Science and Earth Observation (ITC) (2011).
59. S. Baral, R. Malla, and S. Ranabhat, "Above-ground carbon stock assessment in different forest types of Nepal," *Banko Janakari* **19**(2), 10–14 (2010).
60. A. Van Etten, "Quantifying the effects of resolution on image classification accuracy" (2016).
61. P. F. Hsieh, L. C. Lee, and N. Y. Chen, "Effect of spatial resolution on classification errors of pure and mixed pixels in remote sensing," *IEEE Trans. Geosci. Remote Sens.* **39**(12), 2657–2663 (2001).

62. B. A. Baker et al., "Does spatial resolution matter? A multi-scale comparison of object-based and pixel-based methods for detecting change associated with gas well drilling operations," *Int. J. Remote Sens.* **34**(5), 1633–1651 (2012).
63. R. Pouteau, A. Collin, and B. Stoll, "A comparison of machine learning algorithms for classification of tropical ecosystems observed by multiple sensors at multiple scales," in *34th Int. Symp. Remote Sens. Environ.*, pp. 1–6 (2013).

Agbor Esong Effiom is a Cameroonian, with background in environmental science, natural resource management, and geo-information science and Earth observation. He has completed research works in forest and livelihood, including research on combining multispectral Pleiades and UAV images for tree species identification and carbon estimation. Currently, he is teaching at Sakulrajwittayanukul School Sakon Nakhon, Kingdom of Thailand. As a researcher, he is interested in the applications of GIS and remote sensing for forest management, vegetation, and environmental monitoring.

Panagiotis Nyktas is an environmental scientist with an MSc and PhD in physical geography and spatial ecology. His scientific interests lie in geoecology, landscape dynamics, biogeomorphology and Environmental Niche Modelling. He employs GIS, Remote Sensing and photogrammetric methods (UAS) in projects for the conservation of habitats and species in multiple scales. He is motivated to bridge sciences with applied conservation and management of protected areas.

Jefferson Adetokunbo Okojie is currently the program officer for natural resource management at the Environmental and Economic Resource Center, Nigeria. He is simultaneously the chief research officer at GeoNET Research Initiatives, Nigeria. He received his BSc degree in forestry and wildlife management from the Federal University of Agriculture, Abeokuta, and his MSc degree in geoinformation science and earth observation from the faculty of Geoinformation Science and Earth Observation, the University of Twente.

Biographies of the other authors are not available.